Draft version April 18, 2020
Typeset using LaTeX **twocolumn** style in AASTeX63

Future Dynamics of the Local Group

Colin Leach

ABSTRACT

This is a very early draft consisting mostly of placeholders and preliminary ideas. I only pushed it to GitHub so that I wouldn't lose it.

Keywords: Galaxy Merger – Local Group – Stellar Disk – Stellar Bulge – *and more*

1. INTRODUCTION

The largest galaxies in our Local Group (LG) are the Milky Way (MW), Andromeda (M31) and Triangulum (M33). A simulation of MW–M31–M33 orbital evolution was described previously in Marel et al. (2012), hereafter vdM12. That paper included an extensive analysis of both N-body simulations and semi-analytic orbit integrations. The present study uses data from the same N-body simulation to carry out further computational analysis.

The simulation was based on data in vdM12 suggesting that M31 is approaching the MW directly with little proper motion detected by Hubble Space Telescope (HST) studies. Recent data from Gaia DR2 (Brown et al. 2018) suggest that infall is slightly less radial than previously thought (Marel et al. 2019), leading to a slightly later first approach with a larger pericenter distance. However, detailed simulations based on that new data have not yet been carried out.

This paper will review the initial conditions and time evolution for multiple physical parameters of the simulation. Particular attention will be paid to the first MW-M31 close apprach around 4 Gyr, the second approach and merger around 6 Gyr, and the structure and dynamics of the post-merger remnant.

Time probably precludes much analysis of the fate of M33, which will need to be the subject of a future paper.

1.1. *Data*

Data from one N-body simulation in vdM12 was supplied in text-file format by one of the original authors. This included position and velocity data for each particle at the current epoch ($t = 0$) and 800 future time steps. For ease of analysis, this was all transferred to the open source database PostgreSQL[1] (approximately 1.35 billion records). The same database was used to store computed summary data during the analysis.

[1] http://www.postgresql.org

Table 1. Particle counts

Galaxy	DM Halo	Disk	Bulge	Total
MW	250,000	375,000	50,000	675,000
M31	250,000	600,000	95,000	945,000
M33	25,000	46,500	0	71,500
LG	525,000	1,021,500	145,000	1,691,500

Particle counts for each time point are shown in Table 1 and total masses in Table 2. We can see that total mass is the same for MW/M31 but our galaxy has more luminous stars (higher baryon fraction) and M31 has more dark matter (lower baryon fraction). M33 is about 10-fold lighter than either.

Table 2. Aggregate masses ($M_\odot \times 10^{12}$)

Galaxy	DM Halo	Disk	Bulge	Total
MW	1.975	0.075	0.010	2.060
M31	1.921	0.120	0.019	2.060
M33	0.187	0.009	0.000	0.196
LG	4.082	0.204	0.029	4.316

The coordinate system is approximately centered on the Milky Way at $t = 0$. The center of mass (CoM) of all particles in the system is not fixed over time, moving at an average of $\langle 35.9, -26.7, 27.5 \rangle$ km/s with some minor fluctuations due to numerical approximations. In contrast, the total angular momentum of the system is very small at all time points.

1.2. *Software*

The work in this report was carried out in Python using standard packages. Full details are available online[2]

2. RESULTS

2.1. *Trajectories*

The simulation does not explicitly include a supermassive black hole (SMBH) at the center of each galaxy, but the galactic center was defined by calculating the center of mass (CoM) of the disk particles and iteratively constraining the radius of interest until convergence.

To plot motions of the three galactic CoMs it is convenient to transform to a coordinate system in which at $t = 0$ they all lie in the x, y plane with MW and M31 on the x-axis. The overall CoM is moving, as noted above, so at each time point the coordinates are translated to center it at the origin.

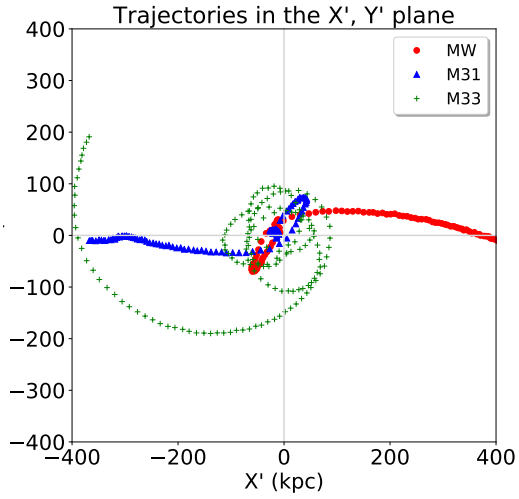

Figure 1. Trajectories of each galactic center of mass in the X',Y' plane. Points are at 71 Myr intervals.

In vdM12 this is referred to as the X',Y',Z' coordinate system and their figure 2 shows multiple views of how the galaxies move through time. In this paper, Figures 1 and 2 show some alternative views in essentially the same coordinates (up to a sign; the x and z axes are flipped). The left panel reproduces the top left panel of vdM12. The right panel shows that MW and M31 remain close to the starting plane while M33 has larger, irregular out-of-plane motions.

[2] Code https://github.com/colinleach/400B_Leach
documentation https://400b-leach.readthedocs.io

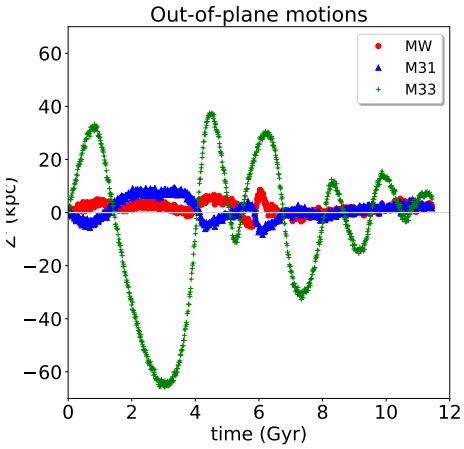

Figure 2. Trajectories of each galactic center of mass perpendicular to the X',Y' plane.

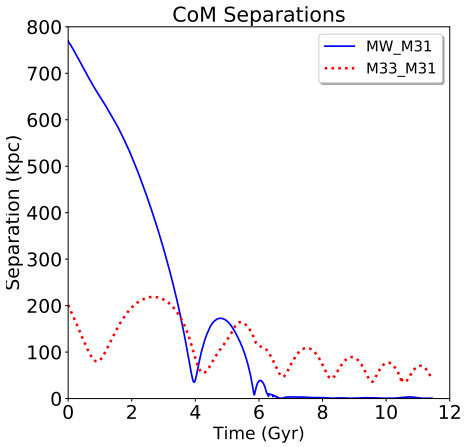

Figure 3. Separations of galactic CoMs.

Relative motions of the CoMs are shown against time in Figures 3 and 4, equivalent to figures 3 and 4 in vdM12.

There is a MW-M31 close approach with first pericenter at 3.96 Gyr with a minimum separation of 35.1 kpc, then a separation to 173 kpc and finally a convergence to 7.8 kpc at second pericenter and merger between 5.9 - 6.5 Gyr. Relative velocities spike sharply during these approaches, as potential energy is converted to kinetic energy, before declining to essentially zero.

Meanwhile, in this simulation run M33 remains separate throughout, albeit on a decaying orbit. In vdM12 the authors investigate the effect of small changes in initial conditions and estimate a 9% chance of an M33-MW collision at first pericenter, before the M31-MW merger.

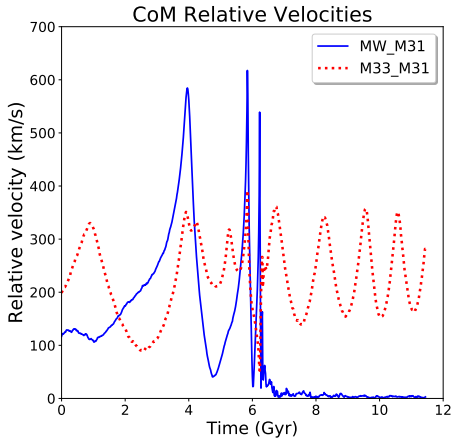

Figure 4. Relative velocities of galactic CoMs.

2.2. *Mass profiles and rotation curves*

Figure 5 shows the cumulative mass profile, by particle type and in total, for each galaxy. The center of each galaxy is dominated by baryonic matter with the DM halo becoming dominant at larger radii.

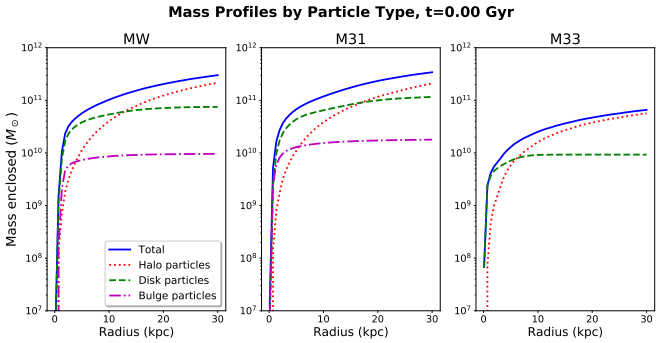

Figure 5. Mass profiles for each galaxy at the current epoch.

Figure 6 shows the rotation curves expected from these mass profiles. Without the DM halo the circular velocity would peak within a few kpc of the CoM then fall steadily at larger radii. With the more diffuse DM halo added, we see the relatively flat overall rotation curves which attracted the attention of astronomers including Zwicky (1933) and Rubin & Ford (1970)

TODO set xlim, make y axis log

2.3. *DM halo*

Figure 6 also adds a theoretical curve in which the dark matter halo is fitted by a Hernquist profile (Hernquist 1990). The cumulative mass out to radius r is given by

$$M(r) = M_h \frac{r^2}{(a+r)^2}$$

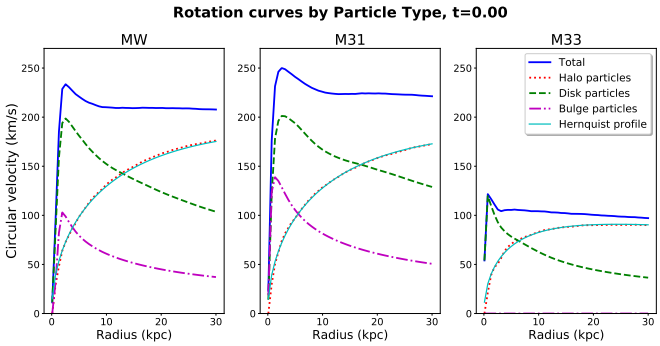

Figure 6. Rotation curves for each galaxy at the current epoch.

where M_h is the total mass of halo particles (see Table 2) and a is a scale radius. Non-linear least squares fitting gave scale radii of 61.1 kpc for MW and M31, 24.3 kpc for M33 at $t = 0$.

Time evolution of the scale radius a is shown in Figure 7. The MW and M31 remain very similar through first pericenter, then start to diverge with MW particles tending to a larger radius than M31. This becomes most pronounced during and after merger. The dissimilar distribution in the merger remnant will be discussed in a later section.

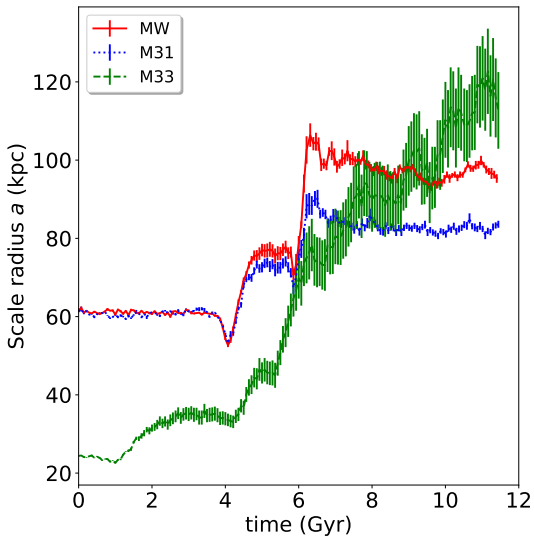

Figure 7. Hernquist scale radius a for DM halo particles originating from each galaxy, with 1σ error bars.

The scale radius for M33 grows inexorably as the original halo is scattered by tidal forces. Figure 7 also shows the increasingly wide error bars for M33: halo particles for this galaxy are no longer well fitted by a Hernquist profile.

TODO identify the bar?

TODO sersic profiles at various stages?

TODO more on spiral arms

2.4. *MW-M31 Close approach*

2.4.1. *Inclinations*

TODO Relative rotation axes of disks – prograde?

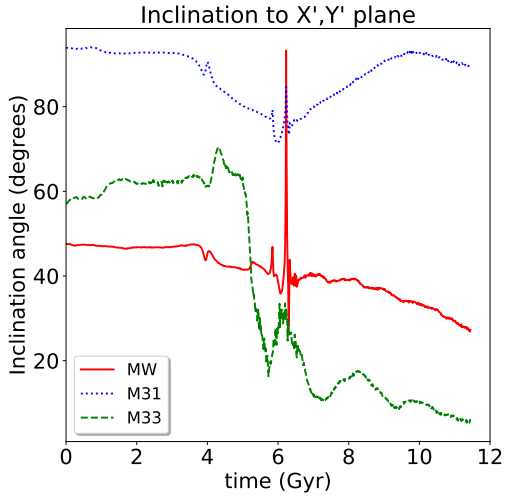

Figure 8. Angular momentum inclination angle to the X',Y' plane for each set of galactic disk particles.

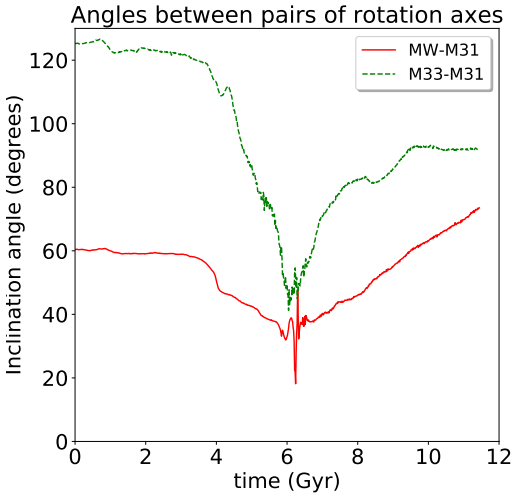

Figure 9. Angular momentum angles between pairs of galaxies.

2.4.2. *Tidal tails and bridges*

The presence of long, symmetrical tails giving some galaxies a distinct 'S'-shape has been described at least as far back as Zwicky (1955). Some astronomers postulated that these were the result of tidal forces during close, glancing encounters, but this was often contested until a detailed computational study by Toomre & Toomre (1972).

In our simulation, both MW and M31 disks remain near-circular during much of the close approach, but conspicuous tails develop as the centers then move further apart. We also see a more sparsely-populated bridge forming between the galaxies.

To determine the nature and origin of stars in this region, a manual selection was performed as in Figure 10. Stars within the yellow rectangle (left panel) are shown with velocity vectors (center panel) and origin (right panel). Velocities are mostly moderate (mean 195 km/s, range 19-586 km/s), with relatively few stars having high kinetic energy.

It appears from the right panel that stars in the tail regions originate in the corresponding disk. The bridge region is more mixed and appears to have a high proportion of former bulge stars. To study this further the coordinate system was transformed to place the large galaxy CoMs on the x-axis at ± 64 kpc, as in Figure 11. It is clear in this view that one MW tail is oriented approximately towards the center of M31.

Table 3. Particle counts close to the midplane

	Bulge	Disk	Total
MW	305	1317	1622
M31	1137	4	1141
Total	1442	1321	2763

The different orientations mean that symmetry about the midplane is imperfect, so the "bridge" region was taken as $-20 < x < 30$ kpc. A count of stars in this region is shown in Table 3. This confirms that the largest populations are MW disk stars (mostly in a relatively dense tail) and M31 bulge stars (more widely dispersed).

TODO identify, trace history, trace fate

TODO Jacobi radius

2.5. *Velocity dispersion*

The changes in velocity dispersion of disk particles originating from each galaxy are shown in 12. The small periodic oscillation seen from the start, especially in M31, appears to be caused by deviations from radial symmetry in the disk: spiral arms and an increasingly prominent bar. Small MW spikes at initial pericenter

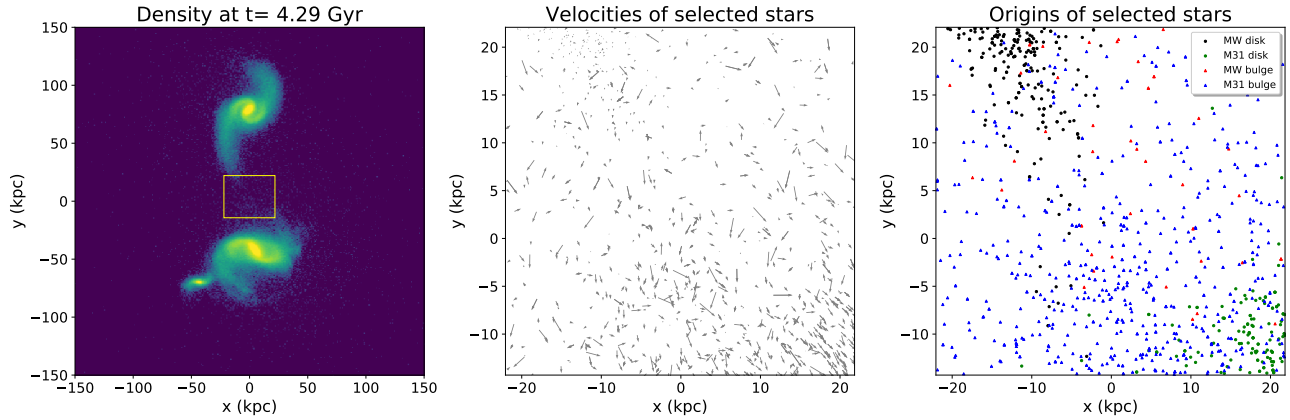

Figure 10. Manual selection of bridge particles at 0.33 Gyr after the first MW-M31 pericenter. The left panel shows stellar surface density and the selected region. The center panel shows velocity vectors for these stars and the right panel shows origin by galaxy and particle type. Orientation is with MW top, M31 bottom and M33 lower left.

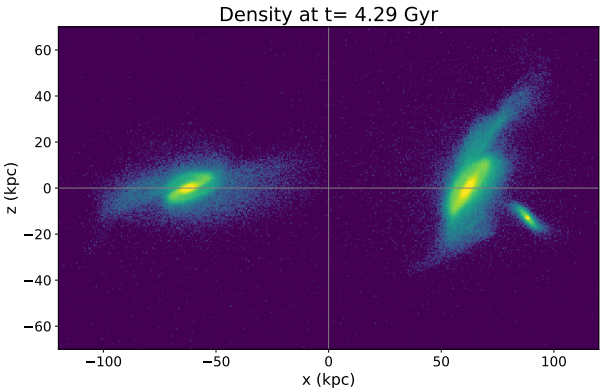

Figure 11. View along the midplane between the galactic centers, MW on the left.

(around 4 Gyr) and much larger ones at merger (around 6 Gyr) are clearly visible.

TODO comment on M33

2.6. *MW-M31 merger*

After second pericenter, the MW and M31 never fully separate and eventually merge. Their mass ratio is 1:1.6 for stellar matter and 1:1 when the DM halo is included. This is thus a 'major merger' in the terminology of TODO ref?. A 1:1 mass ratio has been reported (Boylan-Kolchin et al. 2008; Ji et al. 2014) to lead to the shortest coalescence time.

2.6.1. *Inclinations*

TODO Relative rotation axes of disks – prograde?
TODO expanded 3D trajectories
TODO changes in velocity dispersion
TODO changes in mass profile

2.7. *MW-M31 merger remnant*

TODO shape - how to get principal axes? boxiness?
Refer to Figure 13

2.7.1. *Rotation*

TODO phase diagram
Refer to Figure 14
TODO alignment between particles of different origin?

2.8. *Dark Matter halo*

May need to be split up among previous sections
TODO what happens during close approach? merger? remanant?

REFERENCES

Boylan-Kolchin, M., Ma, C.-P., & Quataert, E. 2008, Monthly Notices of the Royal Astronomical Society, 383, 93, doi: 10.1111/j.1365-2966.2007.12530.x

Brown, A. G. A., Vallenari, A., Prusti, T., et al. 2018, Astronomy & Astrophysics, 616, A1, doi: 10.1051/0004-6361/201833051

Hernquist, L. 1990, The Astrophysical Journal, 356, 359, doi: 10.1086/168845

Ji, I., Peirani, S., & Yi, S. K. 2014, Astronomy & Astrophysics, 566, A97, doi: 10.1051/0004-6361/201423530

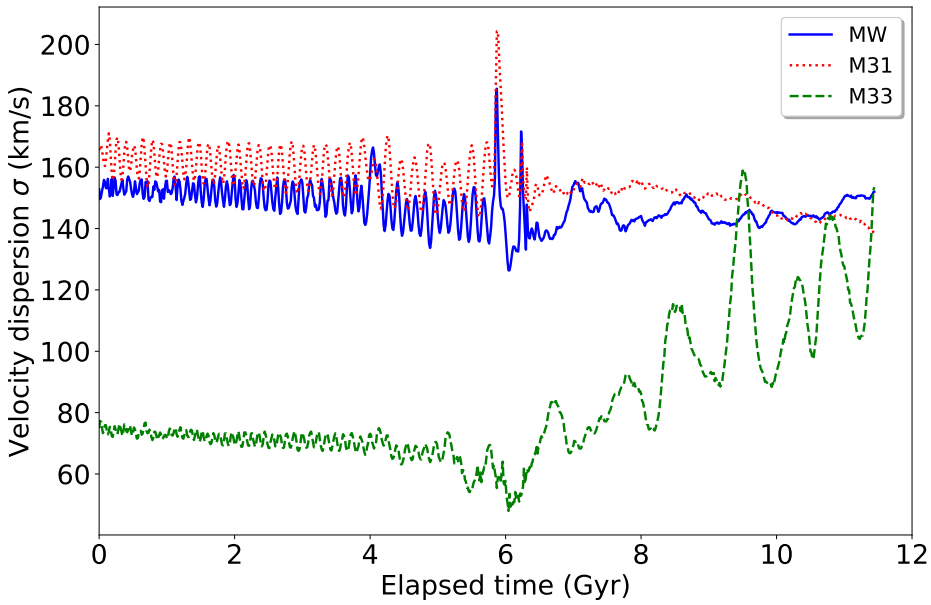

Figure 12. Velocity dispersion of disk particles from each galaxy over time.

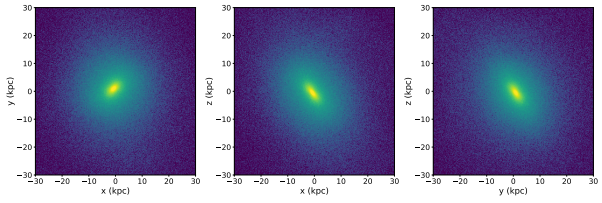

Figure 13. Luminous star density of the MW-M31 remnant in three orthogonal projections.

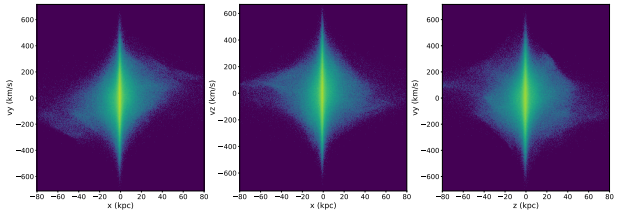

Figure 14. Phase diagrams of the MW-M31 remnant.

Marel, R. P. v. d., Besla, G., Cox, T. J., Sohn, S. T., & Anderson, J. 2012, The Astrophysical Journal, 753, 9, doi: 10.1088/0004-637X/753/1/9

Marel, R. P. v. d., Fardal, M. A., Sohn, S. T., et al. 2019, The Astrophysical Journal, 872, 24, doi: 10.3847/1538-4357/ab001b

Rubin, V. C., & Ford, Jr., W. K. 1970, The Astrophysical Journal, 159, 379, doi: 10.1086/150317

Toomre, A., & Toomre, J. 1972, The Astrophysical Journal, 178, 623, doi: 10.1086/151823

Zwicky, F. 1933, Helvetica Physica Acta, 6, 110. http://adsabs.harvard.edu/abs/1933AcHPh...6..110Z

—. 1955, Publications of the Astronomical Society of the Pacific, 67, 232, doi: 10.1086/126807